



ARTICLE



## Prediction of heterogeneity and anisotropy of oxidised pyrite crystals using electrical measurements

Mohamed Mahmoud Gomaa<sup>a</sup> and Hamed Sedeek<sup>b</sup>

<sup>a</sup>Geophysical Sciences Department, National Research Centre, Cairo, Egypt; <sup>b</sup>Geological Sciences Department, National Research Centre, Cairo, Egypt

### ABSTRACT

Some electrical, geochemical, and mineralogical investigations and analyses were made on some cubic oxidized Pyrite crystals (Gabal El-Sibai). Samples (chemically) are constituted from  $\text{Fe}_2\text{O}_3$ ,  $\text{SiO}_2$ , and  $\text{Al}_2\text{O}_3$ . Electrical features measured at frequency range (100 Hz– 5 MHz). Oxidized Pyrite crystals (cubes) are homogeneous, with no distortion or high variation in their composition. Also, samples have roughly the same structure. Samples were measured in 3-directions. It is supposed that any difference in a lattice structure, in any direction, will be reflected directly in the measurements, i.e. electrical features will attempt to detect variations of homogeneity and anisotropy of samples. The alterations in electrical functions are from mineral composition changes. Changes in texture, at specimens, do not exist (grain size and shape, mineral constituents, and pore throats between grains), and it is supposed that electrical features will be similar in three directions. There were some slight changes in electrical characteristics, due to some imperfections in natural crystals, with some impurities on crystal surfaces that we could not remove. Conductivity rises with frequency increase and accordingly, dielectric constant decreases. The paper aims to prove that the electrical properties, due to homogeneity, are the same at the three perpendicular directions.

### ARTICLE HISTORY

Received 8 November 2020  
Revised 18 January 2021  
Accepted 2 April 2021

### keyword

Electrical properties;  
Dielectric constant;  
Conductivity; Frequency  
domain; pyrite; granite

## 1. Introduction

Shear zones form some mechanical weakness that affects the geology of the continental lithosphere (Butler et al. 1995). Stern and Hedge (1985) and Sultan et al. (1988) recommended that the Najd system covers a larger area at Eastern Desert, Egypt. It controls structure within its central part. Shear zones (Eastern Desert) in the basement of Pan African are associated with extension and compression stresses leading to antiformal structures on a regional scale (Greiling et al. 1993). Gabal El-Sibai (Figure 1) is a double plunge anticline (NW-SE), (Kamal El-Din 1991). Ali (2013) recorded mineralisation within shear zone in the Gabal El-Sebai. Geochemistry of altered minerals about the area of study is limited. The behaviours of elements during hydrothermal and geochemical change are also studied (Yordanov and Kunov 1987).

Börner et al. (2018) study anisotropy and salinity dependence of cores (parallel and perpendicular to the natural Foliation) and crushed samples of black schist and Augen gneiss cores. The study argued the polarisation mechanism to the dissemination of the aligned sheets of graphite. Augen gneiss samples displays weak polarisability and moderate anisotropic conductivity because of the saline solution in the samples. They display that frequency-

dependent conductivity nature and complexity of rocks cannot be eliminated. The parallel (to foliation) black schist cores show low-frequency polarisation. This was present as a peak at complex conductivity and phase shift. The fluid conductivities, composition and porosity of the crushed or core specimens are totally different. Also, there were only one sample of black schist and another one sample of Augen gneiss that were crushed or measured as a core (parallel and perpendicular to the natural Foliation).

Gurin et al. (2018) compared Time Domain Induced Polarisation data for pyrite natural samples with X-ray data. The relationships between chargeability, pyrite concentration and ratio of grain axes (grain anisotropy) were non-linear. That was due to texture, anisotropy and chargeability of some specimens.

Chen and Heidari (2014) displayed that dielectric constant is influenced by texture and concentration of pyrite particles. Clavier et al. (1976) noticed high dependence of electrical measurements on frequency and the apportionment of pyrite particles. The pyrite concentration was small but there was a dependence on frequency of the specimens. The frequency dependence is affected by pyrite concentration and the fluid salinity (Clavier et al. 1976; Misra et al. 2015).

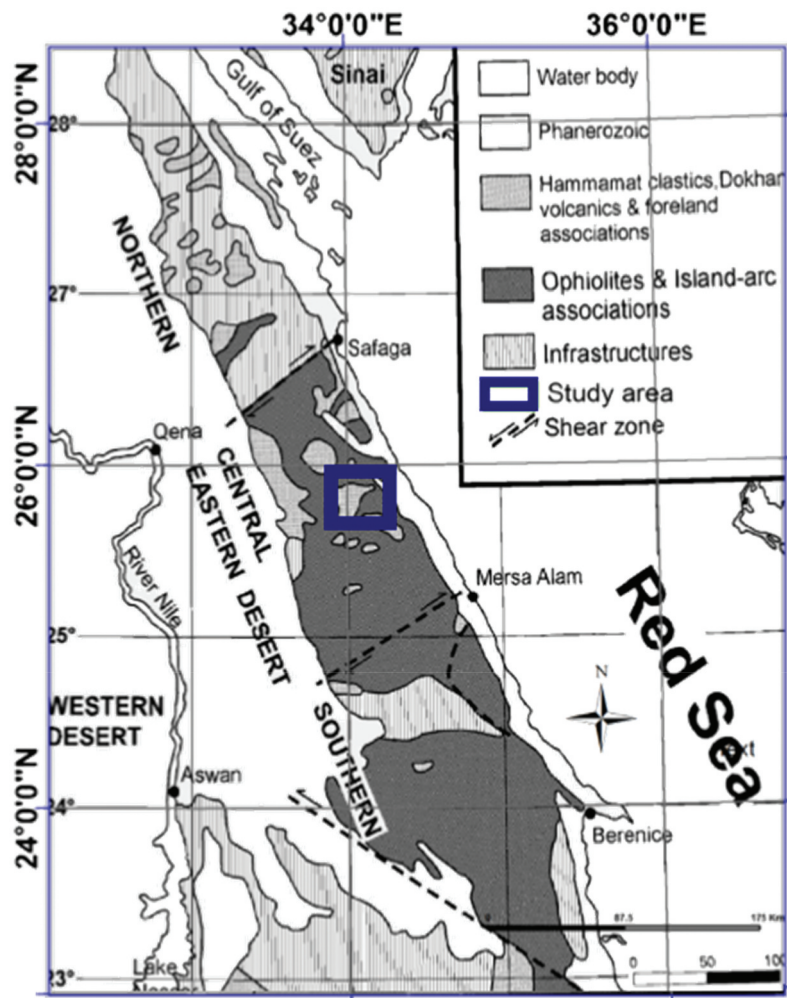


**Figure 1.** Location map of the studied area from Gabal El-Sibai, Egypt.

Dispersed pyrite concentrations in sandstone show a violent increase in conductivity for small pyrite concentration ~5% (Clennell et al. 2010).

Electrical features are, generally, important for frequency spectra interpretation of complex electrical features of rock materials. Also, channels connectivity and measuring of their lengths must be determined.

The cubic oxidised pyrite crystals are semiconductor. Their type and electrical features are defined from their geochemical environment, percentage of the relative quantities and impurities. The electrical features were tested with mineral composition and mineralogy of samples. Our results may help to define homogeneity of crystals using electrical features in three directions (X, Y, Z- dimensions). In oxidised Pyrite crystals, electrically there exists many active impurities as donors (cobalt, nickel, and copper), and other inactive minerals as an acceptor (arsenic) are existed. Sedimentary pyrite deposits are p-type (usually) when no cupriferous sulphide exists. Usually, cubic oxidised pyrite crystals occur in almost any type of geologic environment, so many factors that impact type and density of carrier in specimens are present (Shuey1975).

The potential of cubic oxidised pyrite crystals showed that it is chiefly dependent on solution nature in which it is immersed. The potentials in even dilute ferric sulphate are strikingly high. These results furnish valuable suggestions to interpret these phenomena. When ferric and ferrous salts are present together we are apparently dealing, in part at least, with a “ferrous-ferric” potential. The potential of oxidised Pyrite crystals is plainly affected by changes in the hydroxide or sulphide concentration of alkaline solutions. This record is presenting a marked contrast to that obtained by changes in acid, solutions. The conduction of pyrite resulted from free charge carriers. The sources of free charge carriers are the links between relative quantities of substances taking part in reaction that form the compound. Contribution of the energy gaps, at room temperature, in oxidised pyrite crystals is negligible (0.9 electron volts, Shuey1975). Defects at crystals that produce charge carriers may be donors or acceptors. This is subordinate on the donation of electrons to band conduction or leaving a hole from the acceptance of electrons from valence band. Generally, charge carriers have

one type, unless donors or acceptors concentrations are almost exactly of equal quantity. The resistivity or conductivity (electrical properties) is in relation to charge carriers manufactured mobility and their concentration in samples. For cubic oxidised pyrite crystals no great changes are existed at density of carriers between p-type (positive) and n-type (negative). At structure of cubic oxidised pyrite crystals the anionic types are present as pairs and anion pairs are intense towards the III cubic axes with equal numbers for each axis. This is to preserve the cubic oxidised pyrite symmetry. The electrical features for natural pyrite have distinct values that correspond to minor element concentrations (Ni, Co, and As). Pyrites that have high condensation of Co has high conductivity and high mobility of carrier (n-type semiconductor). Arsenopyrite has low conductivity (p-type semiconductor). These observations may demonstrate the variations between structures of electrons of pyrite arising from impurities, and by the domain distributions with various compositions of impurities that smoothies the movement of electrons. Sedimentary and hydrothermal lower temperature cubic pyrite crystal deposit has p-type conductivity in the absence of Cu. The high temperature tubes of oxidised Pyrite crystals have n-type conductivity in the absence of arsenopyrite (Fleischer 1955; Pridmore and Shuey 1976). As, Co and Ni impurities with different combinations are always present with oxidation of natural pyrite ( $\text{FeS}_2$ ), with other impurities e. g. Pb, Se, Cu and Zn (Shuey 1975; Craig et al. 1998; Abraitis et al. 2004). Electrical features of pyrite (as a semiconductor) depend to some extent on crystal structure defects due to impurity elements (Fe or S) (Rabinovich 1976; Schieck et al. 1990; Lehner et al. 2006). Charge carrier mobility and concentration define the material's conductivity. Replacement of Co and Ni instead of Fe gives some defect states. This replacement may facilitate the electron transfer at the surface and, also, may raise electronic density of band gaps (Chandler and Bene 1973). Pyrite ( $\text{FeS}_2$ ), if it is completely oxidised, is supposed as a semi-conductor mineral. Also, it may change to sulphate and ferrous iron ions. Pyrite oxidation causes loses of seven electrons of each atom. They are converted in pyrite from  $\text{S}^{-1}$  to  $\text{S}^{6+}$  in sulphate ions. Breaking of strong bonds between sulphur and iron produces thiosulphate ions, as an intermediate product. The formed thiosulphate are relatively settled in alkaline electrolytes and unsettled in the acidic electrolytes.

Monitoring electrical features of rocks are useful for exploration of minerals. The electrical features of rocks (conductivity, dielectric constant) are sensible to chemical and physical structure variations, heterogeneity and microstructural factors in samples.

Generally, increase of charge carriers between the substances raises mobility and accordingly the conductivity. The electrical features count on grain shape, grain size and other heterogeneity parameters of specimen (Gomaa 2009; Gomaa et al. 2020).

In this study a trial is given to present some detailed information on geochemistry and electrical features of advanced firriginated alteration and associated altered types. A considerable number of major and trace minerals were analysed, as well as, electrical measurement and their behaviour. Some detailed geochemical, mineralogical, petrographical, electrical information on effect of heterogeneity on electrical features of some oxidised Pyrite crystals within frequency range (100 Hz to 5 MHz) were provided. This study may be extended to a tool for the prediction of grain size anisotropy from electrical properties.

## 2. Geological setting

The cubic oxidised pyrite crystals (Figure 2) are collected from alteration zone of the southern part of Gabal El Sibai granites. These crystals are deep reddish brown colour. Sheared and altered zones are appropriate for circulation of hydrothermal fluids. These granites are considered as intrusive rocks that affected by extrusive dykes and sheared mineralised zone. The intrusive rocks consist of late to post magmatic alkali granites numerous basalt and dolerite and alkaline bostonite dykes represent extrusive dykes (Kamal El Din 1993). They are mainly having the NW-SE direction (Figure 3). There are many different alteration types along this shear zone such as fluoritization, kaolinitization, hematization and silicification which supposed to be a good trap for rare and trace elements. The southern part of Gabal El-Sibai granite, becomes more catalase and mylonitised especially along the shear zone. The shear zone mineralised part varies in length (50–300 m) and width (0.3–2 m), at front of the granite alkali feldspar.

## 3. Methodology

Some specimens were collected, of the cubic oxidised pyrite, from south El-Sebai shear zone, in Qusseir area southern part (Figure 2). Samples were studied mineralogically by PAN analytical X-ray diffraction technique (Egyptian Mineral Resources Authority, Egypt). X'Pert PRO model was used with secondary monochromator. Cu-radiation ( $\lambda = 1.542 \text{ \AA}$ ) at 45 K. V., 35 M. A, with scanning speed  $0.02^\circ/\text{s}$ . The diffraction patterns and intensities were compared with ICDD data. Morphology and size samples were described using SEM and EDX (SEM Model Quanta FEG 250), at National Research Centre. The chemical constituents of some samples were determined using an Axios





was used for these electrical features measurements. Electrode area size was chosen to be smaller than the sample area to avoid fringing effect. The electrodes used were Cu/CuSO<sub>4</sub> to enhance the contact of the electrode with the sample (more details of the measurements and methodology are present at Gomaa and Alikaj 2009).

## 4. Results and discussion

### 1) Mineralogy

Mineralogical nature of oxidised cubic pyrite was identified by using X-ray diffraction (XRD) analyses. Investigation XRD analysis displayed two mineral phases in the studied cubic oxidised pyrite samples of Gabal El-Sibai alteration shear zone in granites. Goethite is the main mineral with some arsenopyrite (Figure 4). The enrichment of iron oxide discloses that the studied oxidised cubic pyrite samples contain significant quantities of iron. Some authors mentioned

that the main iron mineral in the Gabal El-Sibai alteration shear zone is due to hydrothermal solution (Ali 2013). Also, the X-ray diffraction patterns confirm the geochemical studies and show very sharp and narrow peaks (Figure 4), which are reflecting high crystallinity of the identified goethite. SEM and EDX examination of the oxidised cubic pyrite sample showed the dominance of radial and euhedral forms (Figure 5 and Figure 6). The obtained EDX data show the accumulation of high condensation of Fe and Nd (%). This indicates that cubic oxidised pyrite samples have goethite bearing Agardite, which is confirmed with XRD.

### 2) Geochemistry

The six samples selected for geochemical study (trace and major elements) are present in (Table 1), Table (2), Table (3) and Table (4). Tables show that cubic oxidised pyrite samples are composed mainly of Fe<sub>2</sub>O<sub>3</sub>, SiO<sub>2</sub>. The loss of ignition (H<sub>2</sub>O) ranges from 6.81% to 11.10% and Al<sub>2</sub>O<sub>3</sub> ranges from 3.56% to 8.51%.

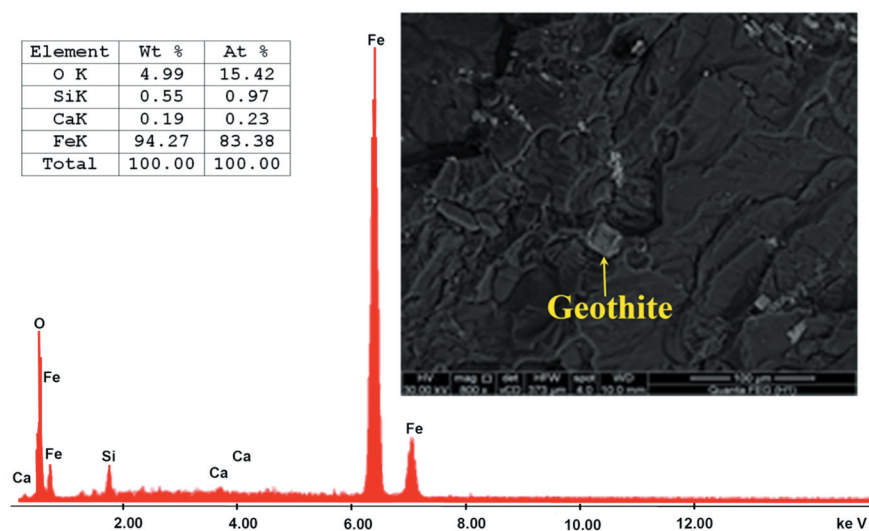


Figure 4. SEM-EDX spectra, BSE images and microanalyses of goethite.

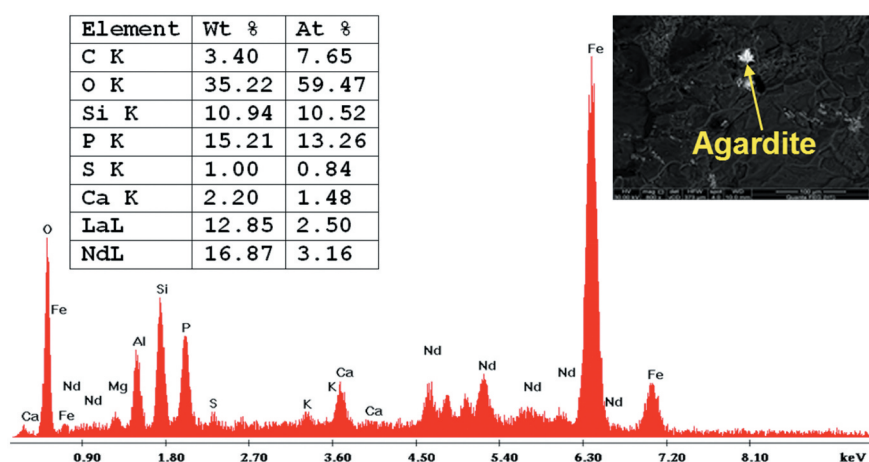
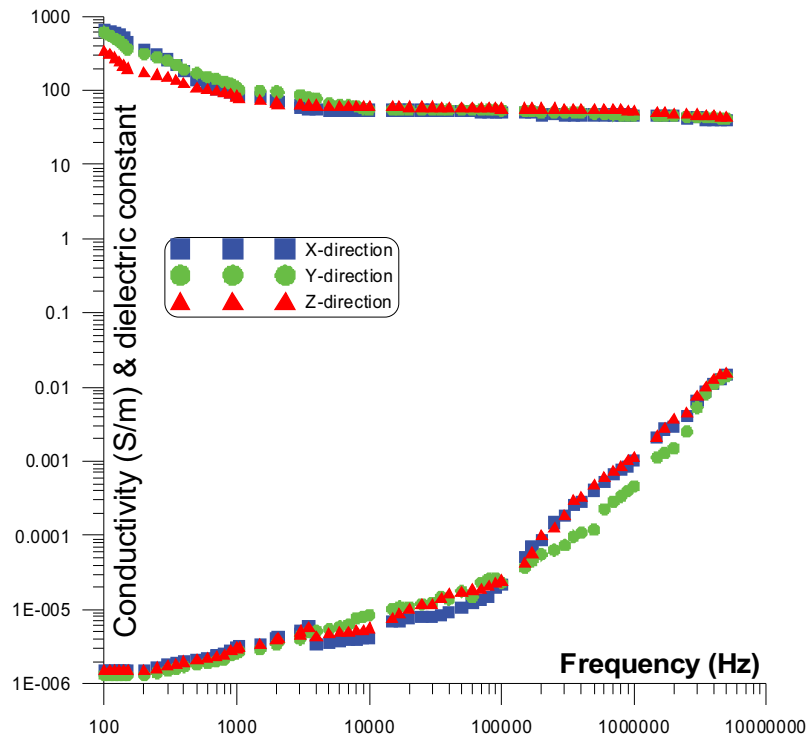
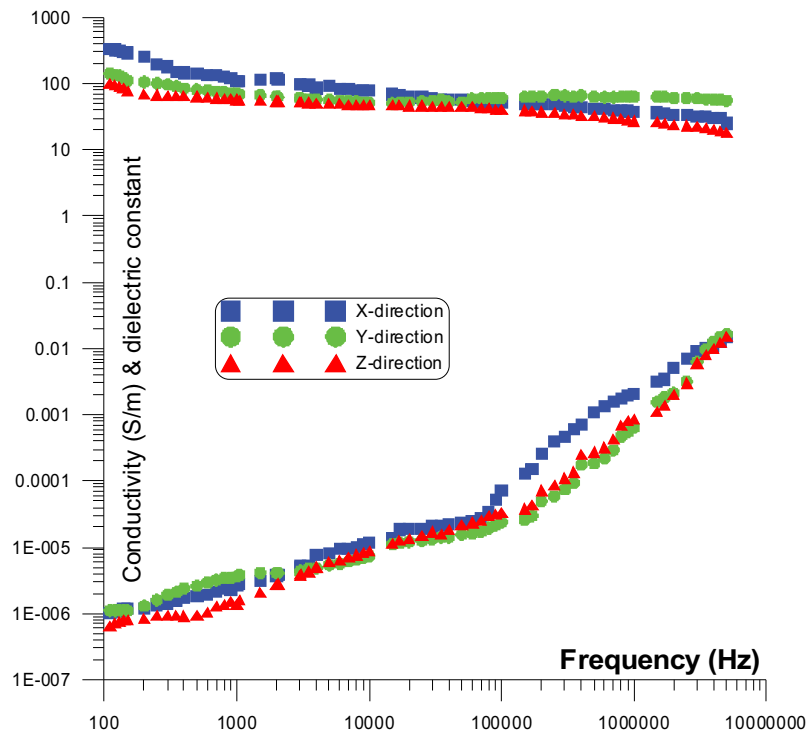


Figure 5. SEM-EDX spectra, BSE images and microanalyses of Agardite.



**Figure 6.** The conductivity and dielectric constant of pyrite sample (1) at three directions (X, Y and Z) of the crystal.



**Figure 7.** The conductivity and dielectric constant of pyrite sample (2) at three directions (X, Y and Z) of the crystal.

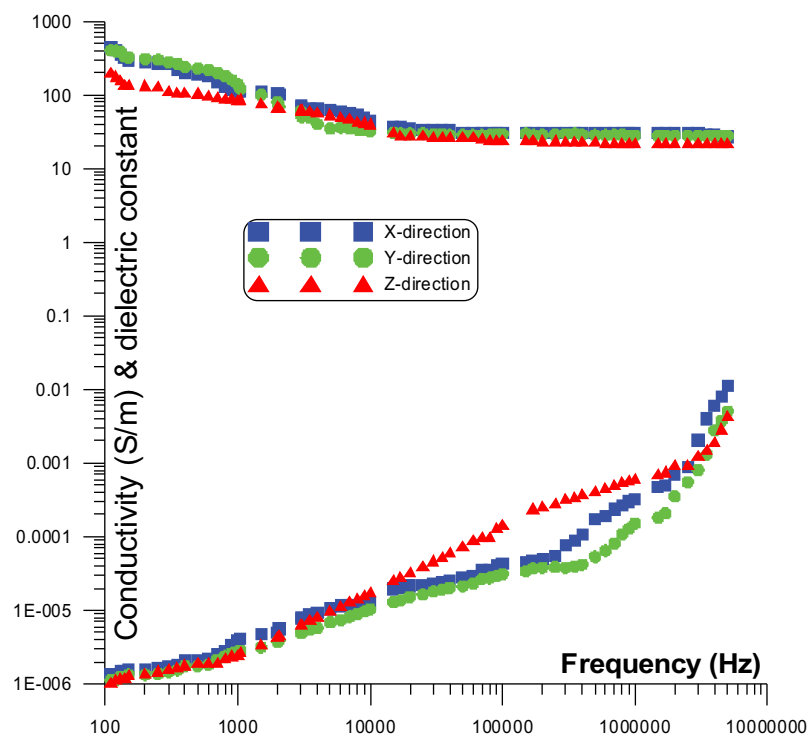


Figure 8. The conductivity and dielectric constant of pyrite sample (3) at three directions (X, Y and Z) of the crystal.

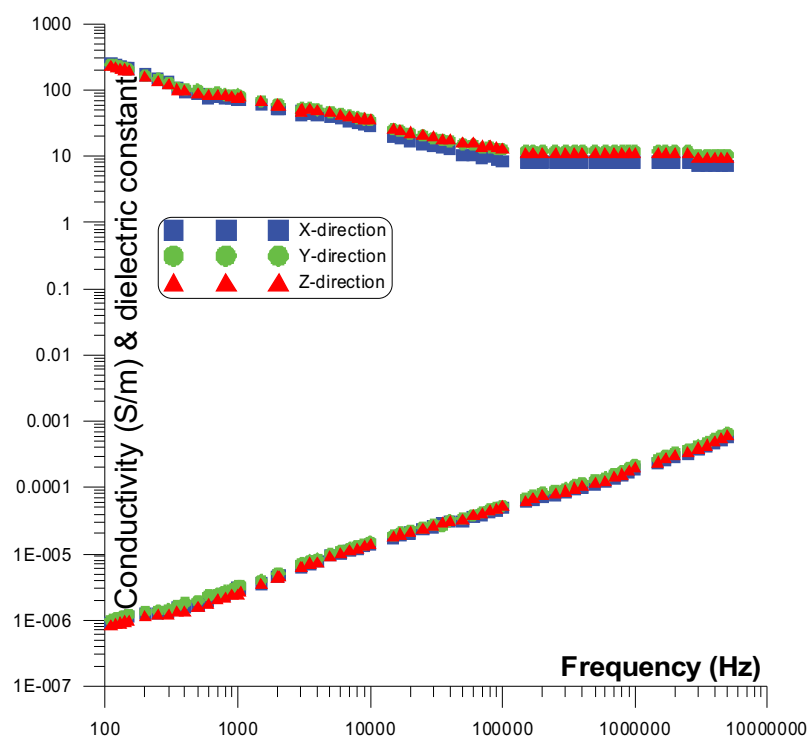
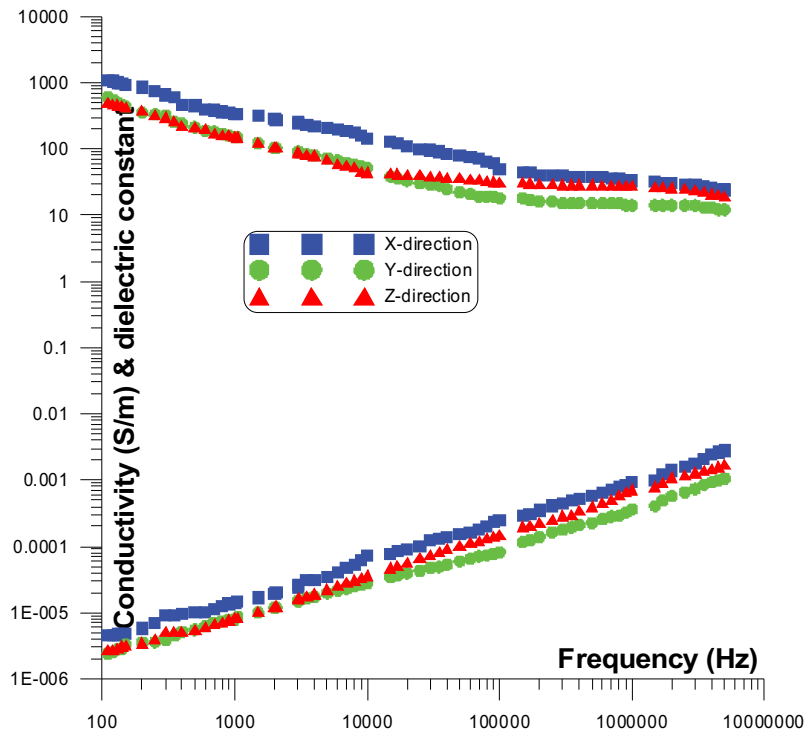


Figure 9. The conductivity and dielectric constant of pyrite sample (4) at three directions (X, Y and Z) of the crystal.



**Figure 10.** The conductivity and dielectric constant of pyrite sample (5) at three directions (X, Y and Z) of the crystal.

**Table 1.** XRF data major (%) elemental ratios of selected studied samples in cubic oxidised pyrite of Gabal El-Sibai granites.

Element	Sample Name					
	1	2	3	4	5	6
Fe <sub>2</sub> O <sub>3</sub>	52.315	38.515	66.066	67.815	57.466	60.932
SiO <sub>2</sub>	26.095	38.98	13.245	13.281	20.99	18.528
Al <sub>2</sub> O <sub>3</sub>	5.646	8.517	4.46	3.565	4.787	5.549
K <sub>2</sub> O	2.656	4.038	2.123	1.379	2.43	2.442
CaO	1.246	0.897	0.933	0.72	1.276	1.887
SO <sub>3</sub>	1.891	0.407	0.299	0.682	0.452	0.448
MgO	0.274	0.407	0.278	0.298	0.513	0.342
TiO <sub>2</sub>	0.186	0.345	0.28	0.376	0.331	0.18
P <sub>2</sub> O <sub>5</sub>	0.207	0.17	0.242	0.159	0.222	0.251
Na <sub>2</sub> O	0.127	0.19	0.146	0	0.163	0.119
H <sub>2</sub> O	8.9	6.81	8.87	10.72	11.04	11.1

#### 4.1. Major elements

The dominant major oxides are Fe<sub>2</sub>O<sub>3</sub> that ranges from 38.51 to 67.81% and SiO<sub>2</sub> oxides ranges from 13.24 to 38.98%. There is another appreciable amounts of K<sub>2</sub>O (from 1.37% to 4.03%), and CaO (from 0.72 to 1.88%). Also, there is another minor trace of other oxides such as SO<sub>3</sub> (from 0.29 to

**Table 2.** XRF data trace elements (ppm) elemental ratios of selected studied samples in cubic oxidised pyrite of Gabal El-Sibai granites.

Element	Sample Name					
	1	2	3	4	5	6
As	120.7	63.1	113.7	137.4	83.3	91.9
Ba	2378.8	1808.2	2144.7	1628.8	2256.9	2345.3
Cu	33.9	22.1	45	48	31.1	43
Ga	16.7	23.7	33.7	10.2	22.2	17.7
Mn	3013.6	1333.3	6021.6	4853.6	4259.5	4090.7
Mo	489.6	331.5	697.4	831.3	589	495.1
Nb	45.4	62.8	82.5	89.6	80	39.6
Ni	66	41.2	107.7	112.1	96.2	86.1
Pb	25.9	10.4	30.9	39.1	19.9	26.2
Rb	88.9	113.3	62.6	43.7	80	71.2
Sr	497.9	287.6	695.7	411	325.7	848.5
Th	55.8	32.6	16.6	58.4	46	13.3
U	18.1	14.7	32.6	36.6	15.4	27.1
Zn	221.1	129.5	225.9	269.3	220.8	191.1
Zr	890.2	1010.7	1572.6	1738.1	1396.2	624.9

1.89%), MgO (from 0.27 to 0.51%), TiO<sub>2</sub> (from 0.18 to 0.37%), P<sub>2</sub>O<sub>5</sub> (from 0.15 to 0.25%) and Na<sub>2</sub>O (from 0.00 to 0.19%). Trace and rare elements that were detected are present at (Table 1) in ppm.

**Table 3.** XRF data rare elemental ratios of selected studied samples in cubic oxidised pyrite of Gabal El-Sibai granites.

Element	Sample Name					
	1	2	3	4	5	6
Ce	1458.5	756.9	2764.7	2010.6	1050.5	3124.1
La	1161	445.6	1921.5	2173.9	807.6	2223.4
Nd	925	373.1	1340.4	1980.7	676.6	1344.5
Sm	124.2	120	38.1	278.7	68.9	198.9
Y	176.1	160.8	270.1	318.2	278	158.7

#### 4.2. Trace elements

Concentration of trace elements are Ba (1628.8 to 2378.8 ppm), Zr (624.9 to 1738.1 ppm), Mo (331.5 to 831.3 ppm), Sr (287.6 to 848.5 ppm), Zn (129.5 to 269.3 ppm), As (63.1 to 137.4 ppm), Rb (43.7 to 113.3 ppm), Ni (41.2 to 112.1 ppm), Nb (39.6 to 89.6 ppm), Th (13.3 to 58.4 ppm), Cu (22.1 to 48 ppm), Pb



**Table 4.** Correlation coefficients of the major and trace elements in the studied cubic oxidised pyrite.

	Fe <sub>2</sub> O <sub>3</sub>	SiO <sub>2</sub>	Al <sub>2</sub> O <sub>3</sub>	K <sub>2</sub> O	CaO	SO <sub>3</sub>	MgO	TiO <sub>2</sub>	P <sub>2</sub> O <sub>5</sub>	Na <sub>2</sub> O	H <sub>2</sub> O	As	Ba	Ce	Cu	Ga	La
Fe <sub>2</sub> O <sub>3</sub>	1																
SiO <sub>2</sub>	-0.996	1															
Al <sub>2</sub> O <sub>3</sub>	-0.905	0.903	1														
K <sub>2</sub> O	-0.921	0.9	0.967	1													
CaO	0.001	-0.002	0.005	0.006	1												
SO <sub>3</sub>	0.025	0.026	0	0	0.003	1											
MgO	-0.139	0.126	0.077	0.136	0.025	-0.172	1										
TiO <sub>2</sub>	0.001	0.002	-0.004	-0.003	-0.599	-0.231	0.147	1									
P <sub>2</sub> O <sub>5</sub>	0.107	-0.141	-0.039	-0.015	0.527	-0.023	0	-0.464	1								
Na <sub>2</sub> O	-0.449	0.39	0.481	0.641	0.059	-0.024	0.231	-0.038	0.141	1							
H <sub>2</sub> O	0.803	-0.821	-0.907	-0.801	-0.039	-0.021	-0.016	0.047	0.051	-0.258	1						
As	0.537	-0.508	-0.624	-0.698	-0.079	0.19	-0.535	-0.005	-0.012	0.424	0.424	1					
Ba	0.001	-0.006	0	0.003	0.6	0.111	0.002	-0.695	0.699	0.205	0	-0.014	1				
Ce	0.521	-0.523	-0.245	-0.308	0.169	-0.051	-0.314	-0.225	0.375	0.126	0.15	0.174	0.062	1			
Cu	0.895	-0.869	-0.706	-0.809	0.001	-0.009	-0.363	-0.016	0.066	-0.562	0.524	0.616	-0.003	0.833	1		
Ga	0.01	0.003	0.043	0.099	-0.008	-0.187	0.009	0	0.245	0.497	0.001	-0.143	0.062	0.008	-0.032	1	
La	0.733	-0.703	-0.485	-0.615	0.037	-0.016	-0.383	-0.063	0.093	-0.496	0.294	0.451	0	0.833	0.935	-0.049	1
Mn	0.888	-0.926	-0.792	-0.731	-0.001	-0.074	-0.089	0	0.206	-0.189	0.853	0.37	0.01	0.467	0.721	0.044	0.535
Mo	0.899	-0.783	-0.865	-0.881	-0.148	-0.016	-0.105	0.122	-0.005	-0.591	0.843	0.628	-0.101	0.168	0.679	-0.031	0.445
Nb	0.172	-0.166	-0.241	-0.198	-0.572	-0.195	0.022	0.727	-0.128	-0.099	0.443	0.075	-0.372	-0.021	0.065	0.029	0.003
Nd	0.757	-0.704	-0.632	-0.787	-0.013	-0.001	-0.371	0.001	0	-0.815	0.417	0.688	-0.079	0.481	0.913	-0.156	0.854
Ni	0.937	-0.94	-0.909	-0.873	-0.027	-0.077	-0.032	0.031	0.069	-0.363	0.923	0.409	-0.003	0.325	0.719	-0.001	0.518
Pb	0.818	-0.781	-0.789	-0.893	0.027	0.016	-0.409	-0.001	0	-0.751	0.577	0.871	-0.025	0.392	0.892	-0.113	0.738
Rb	-0.914	0.909	0.87	0.946	0.012	0.022	0.163	-0.015	-0.01	0.666	-0.727	-0.616	0.035	-0.418	-0.899	0.068	-0.742
Sm	0.067	-0.04	-0.053	-0.15	0	0.011	-0.083	0.012	-0.231	-0.675	0	0.196	-0.233	0.046	0.177	-0.766	0.256
Sr	-0.272	-0.272	-0.079	-0.104	0.384	-0.009	-0.264	-0.517	0.585	-0.01	0.028	0.056	-0.255	0.886	0.399	0.31	0.562
Th	-0.022	0.005	-0.054	-0.052	-0.203	0.366	0.001	0.121	-0.465	-0.199	0.026	0.177	-0.088	-0.36	-0.015	-0.409	-0.069
U	0.703	-0.662	-0.495	-0.623	-0.049	-0.056	-0.407	0.011	0.001	-0.582	0.385	0.531	-0.125	0.563	0.881	-0.016	0.829
Y	0.477	-0.468	-0.622	-0.56	-0.308	-0.071	0.001	0.405	-0.041	-0.296	0.78	0.287	-0.173	0.003	0.267	-0.002	0.097
Zn	0.749	-0.725	-0.929	-0.916	-0.043	0.051	-0.127	0.009	-0.06	-0.586	0.794	0.784	-0.002	0.116	0.591	-0.116	0.367
Zr	-0.267	-0.258	-0.364	-0.321	-0.599	-0.085	-0.001	0.571	-0.121	-0.186	0.553	0.214	-0.326	-0.004	0.144	0.012	0.028
V	0.261	-0.295	-0.148	-0.095	0.063	-0.582	0.119	0.009	0.419	0.03	0.292	-0.033	0.047	0.217	0.115	0.288	0.094
Se	0.495	-0.454	-0.521	-0.654	0.036	0.133	-0.253	-0.063	-0.05	-0.772	0.228	0.646	0	0.27	0.599	-0.518	0.591
Mn	1							Sm	Sr	Th	U	Y	Zn	Zr	V	Se	
Mo	0.718	1						0.003	1	-0.019	1	1					
Nb	0.252	0.504	1					0.107	-0.481	0.134	0.298	1	1				
Nd	0.504	0.709	0.095	1				0.223	-0.056	0.206	0.422	0.609	1				
Ni	0.91	0.857	0.356	0.604	1			0.09	-0.127	0.117	0.251	0.898	0.389	1			
Pb	0.606	0.122	0.924	0.924	0.676	-0.898	1	0	0.153	-0.369	0.073	0.151	0.019	0.078	1		
Rb	-0.755	-0.891	-0.232	-0.889	-0.885	-0.233	-0.196	0.008	0.056	0.112	0.401	0.092	0.584	0.008	-0.018	1	
Sm	-0.002	0.093	-0.004	0.402	0.025	0.233	-0.149	0.223	-0.056	0.134	0.298	0.609	1				
Sr	0.246	0.014	-0.185	0.201	0.108	0.159	-0.007	0.09	-0.127	0.117	0.251	0.898	0.389	1			
Th	-0.036	0.069	0.073	0.006	0	0.039	-0.803	0.008	0.056	0.112	0.401	0.092	0.584	0.008	-0.018	1	
U	0.57	0.667	0.159	0.901	0.58	0.796	-0.007	0.223	0.247	-0.019	1	1	1				
Y	0.503	0.814	0.838	0.301	0.684	0.388	-0.544	0.008	-0.056	0.134	0.298	0.609	1				
Zn	0.588	0.841	0.235	0.605	0.731	0.808	-0.771	0.09	-0.127	0.117	0.251	0.898	0.389	1			
Zr	0.341	0.65	0.956	0.186	0.443	0.253	-0.342	0	-0.127	0.117	0.251	0.898	0.389	1			
V	0.444	0.106	0.13	0.019	0.366	0.012	-0.141	-0.133	0.153	-0.369	0.073	0.151	0.019	0.078	1		
Se	0.208	0.383	-0.003	0.705	0.327	0.71	-0.585	0.531	0.147	0.112	0.401	0.092	0.584	0.008	-0.018	1	

(10.4 to 39.1 ppm), U (14.7 to 36.6 ppm) and Ga (10.2 to 33.7 ppm) (Table 2).

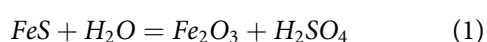
### 4.3. Rare earth elements

Concentrations of rare elements are Ce (756.9 to 3124.1 ppm), La (445.6 to 2223.4 ppm), Nd (373.1 to 1980.7 ppm), Y (158.7 to 318.2 ppm) and Sm (38.1 to 278.8 ppm) (Table 3).

High values of loss on ignition of oxidised pyrite revealed that the aqueous medium at hydrothermal solution is the dominant condition environment for precipitation of oxidised Pyrite crystals. The existence of haematite and goethite minerals in the absence of pyrite as determined by XRD are the result from oxidation of pyrite crystals by the hydrothermal solution elements rich in iron (FeO) that penetrates the bearing area of this pyrite metal.

Negative correlation between  $\text{Fe}_2\text{O}_3$  and  $\text{SiO}_2$  ( $r = -0.996$ ),  $\text{K}_2\text{O}$  ( $r = -0.921$ ),  $\text{Al}_2\text{O}_3$  ( $r = -0.905$ ) and high correlation between  $\text{Fe}_2\text{O}_3$  with  $\text{H}_2\text{O}$  ( $r = 0.803$ ). Very weak correlation with  $\text{SO}_3$  ( $r = 0.025$ ) may show that most Fe is present as oxide mineral (goethite). This is confirmed with X-ray diffraction (Figure 4). Also, the existence of hydrothermal solution was confirmed by SEM and EDX examination (Figure 5).

There is a high positive correlation between  $\text{Fe}_2\text{O}_3$  and Ni (0.937), Mn (0.899), Cu (0.895), Mo (0.888), Pb (0.818), Zn (0.749), U (0.703), La (0.733) and Nd (0.757), with a strong negative correlation with Rb ( $r = -0.914$ ). Low content of  $\text{SO}_3$  ranges from 0.299 to 1.891% and very weak correlation with  $\text{Fe}_2\text{O}_3$  ( $r = 0.025$ ) could be the result of alteration of pyrite to iron oxide and sulphuric acid



Thus, the result is the forming of cubic iron oxide, this confirms the lack of a relationship between  $\text{SO}_3$  and  $\text{Al}_2\text{O}_3$  (0),  $\text{K}_2\text{O}$  (0), CaO (0.003) and  $\text{SiO}_2$  (0.026). High correlation between  $\text{SiO}_2$  and  $\text{Al}_2\text{O}_3$  (0.903),  $\text{K}_2\text{O}$  (0.9) revealed that most  $\text{SiO}_2$  are exist as alkali feldspar mineral which was confirmed from the geological study of (Ali 2013).

Samples of the oxidised pyrite are enriched with some trace elements of Mn (~3928 ppm), Ba (~2093 ppm), Zr (~1205 ppm), Mo (~572 ppm), Sr (~511 ppm) and Zn (~209 ppm). Also, pyrite samples are enriched with some rare earth minerals of Ce (~1860 ppm), La (~1455 ppm), Nd (~1106 ppm), Y (~226 ppm) and Sm (~138 ppm), which is in accordance with obtained EDX data. These crystals are characterised by the existence of Agardite.

Ni, Mn, Cu, Mo, Pb, Zn, U, Nd and La have a strong to moderate good correlation with both  $\text{Fe}_2\text{O}_3$  ( $r = 0.937, 0.899, 0.895, 0.888, 0.818, 0.749, 0.703, 0.758$  and  $0.733$ ) and  $\text{H}_2\text{O}$  ( $r = 0.923, 0.853, 0.524,$

$0.843, 0.577, 0.794, 0.385, 0.417$  and  $0.294$ ) respectively. This shows that trace minerals are associated with hydrothermal solution. The strong positive correlation between Rb and  $\text{SiO}_2$  (0.909),  $\text{Al}_2\text{O}_3$  (0.87),  $\text{K}_2\text{O}$  (0.946) and  $\text{Na}_2\text{O}$  (0.666) reveals that Rb was associated with some alkali feldspar minerals.

The most available trace element in specimens is manganese (~3928 ppm). High condensation of Mn with positive correlation with  $\text{Fe}_2\text{O}_3$  (0.899),  $\text{H}_2\text{O}$  (0.853), Cu (0.721), Ni (0.91), Mo (0.718), Pb (0.606), Zn (0.588) and U (0.57) are exist. Also, negative correlation with  $\text{SiO}_2$  (-0.926),  $\text{Al}_2\text{O}_3$  (-0.792),  $\text{K}_2\text{O}$  (-0.731) and Rb (-0.755) are existed. This is due to the oxidation and transition during hydrothermal solution. Also, it may be resulted from ferrugination associated with the kaolinitization and silicification procedures. High ability of iron oxides to adsorb radioactive elements from its solutions may exist. The ferrugination procedures resulted from mobility of ferric ions liberated from the ferromagnesian minerals during the alteration procedures (Ali 2013). Quinby-Hunt and Wilde (1994) agree with this idea, where they investigated that high condensation of Mn represents an oxic condition, while less than 260 ppm is considered an anoxic environment. Thus the enrichment of Mn (~3928 ppm) display that specimens are deposited under toxic conditions.

Barium represents the second most abundant trace element in specimens (~2093 ppm) and it shows good correlation with  $\text{P}_2\text{O}_5$  (0.699),  $\text{TiO}_2$  (0.695) and CaO (0.6). The high content of zirconium (~1205 ppm) and the high correlation with Nb (0.956), Y (0.888) and  $\text{TiO}_2$  (0.57) reveal that it is combined with haematite during the alteration processes.

Immobile elements like Fe, Ti, Cr, Co, Cu, Ga, Sc, Pd, Th, Nb, Zr and Y are used for both classifications of magmatic and metamorphic rocks. It may also be used for discrimination of hydrothermally modified rocks (MacLean and Kranidiotis 1987). Some elements like Ti, Zr, Y, Nb, Ce, Ga, Sc, are supposed to be stationary during the alteration procedures (Fedot et al. 1996). Taylor and McLennan (1985) reported that Al, Fe, Ti, Cr, Th, Pd, Nb, Sc, Co, Zr, Y, Ga and Se are commonly immobile elements and good markers of source, such as weathering, movement and sorting. Thus the good correlations between  $\text{TiO}_2$  and Zr, Nb, Y (Table 2) reveal that these elements are concentrated during weathering processes.

Studied specimens contain different concentrations of Mo (~572 ppm), Sr (~511 ppm), Zn (~209 ppm). These elements have a marked high correlation with  $\text{Fe}_2\text{O}_3$  and  $\text{TiO}_2$  while negative correlation between Rb and  $\text{Fe}_2\text{O}_3$  and  $\text{TiO}_2$  may exist. This means that during weathering processes, these elements might have been modified or were subjected to weathering conditions that affect concentrations of these elements.

It is interesting to note that the low concentration of  $\text{SO}_3$  in the oxidised pyrite samples of Gabel El-Sebai granites is similar to that of high-temperature hydrothermal fluids. It is different at sedimentary fluids, suggesting that the similar growths are resulted from high-temperature hydrothermal fluids in a heat reaction zone and/or rocky near geological structures. However, Shen-Xubao and Iao-Tongpeng (2008) shows that sulphate concentration are faint at high-temperature fluids excluding the fluids of Gremlin opening.

Shannon (1976) suggested that REE and Y are still tied in several geochemical procedures and orderly changes in their chemical properties. These procedures resulted from decrease of radius of ions of trivalent REE with adding to atomic number.

Shen-Xubao et al. (2008) investigated that sulphate concentration are little in most fluids of high temperature excluding the fluids of Gremlin opening, they also show that REE are mixed with sulphate that created from oxidation of magmatic  $\text{SO}_2$  and  $\text{H}_2\text{S}$  in Gremlin. The low concentration of  $\text{SiO}_3$  content at specimens indicates the presence of fluids with high temperature for the cubic oxidised pyrite of south Gabal El-Sibai shear zone. Also, high condensation of Ce (~1860 ppm), La (~1455 ppm), Nd (~1106 ppm), Sm (~138 ppm) and Y (~226 ppm) revealed that the loss of  $\text{SiO}_3$  is resulted from hot hydrothermal solution at shear zone which bearing dissented cubic pyrite.

Thus the loss of pyrite at studied specimens display no relation between  $\text{SO}_3$  with Ce (−0.051), La (−0.016), Nd (−0.001) Sm (0.011) and Y (−0.071).

High correlation between La and Ce ( $r = 0.833$ ), La and Nd ( $r = 0.854$ ) revealed that the high Ce, La, Nd, Y and Sm contents, accumulated in cubic oxidised pyrite, under hot hydrothermal fluid condition are gradually increased in oxidation processes.

### 3) Electrical measurements

The changes of conductivity and permittivity with frequency, of the cubic oxidised pyrite crystals, at three directions (X, Y and Z), are presented at (Figures 6,7,8,9,10, and 11). There is a general increase of conductivity in the cubic oxidised pyrite samples with the raise of frequency, free charge carriers and raise of excitation across energy gaps that will increase the continuous conduction paths. The main conductor concentration in samples is  $\text{Fe}_2\text{O}_3$  content while the main insulator concentration in samples is the  $\text{SiO}_2$  content. The average of conductivity values in all samples, at relatively low frequency (100 Hz), ranges from  $5 \times 10^{-6}$  to  $7 \times 10^{-7}$  (S/m). In our case, samples are homogeneous (have nearly the same texture and concentration) in spite of they are taken from different locations. Also, the average changes of the conductivity values at the different samples, are so small and could be negligible, when measured at three directions (X, Y and Z) of the crystal. This also indicates that samples are homogeneous and there is no anisotropy at specimens because of perfect cubic symmetry of specimens. The summation of the different conductor conduction links at specimens gives total conductor concentrations. Accordingly, with the increase of conductor conduction links between electrodes, the impedance at specimens increases.

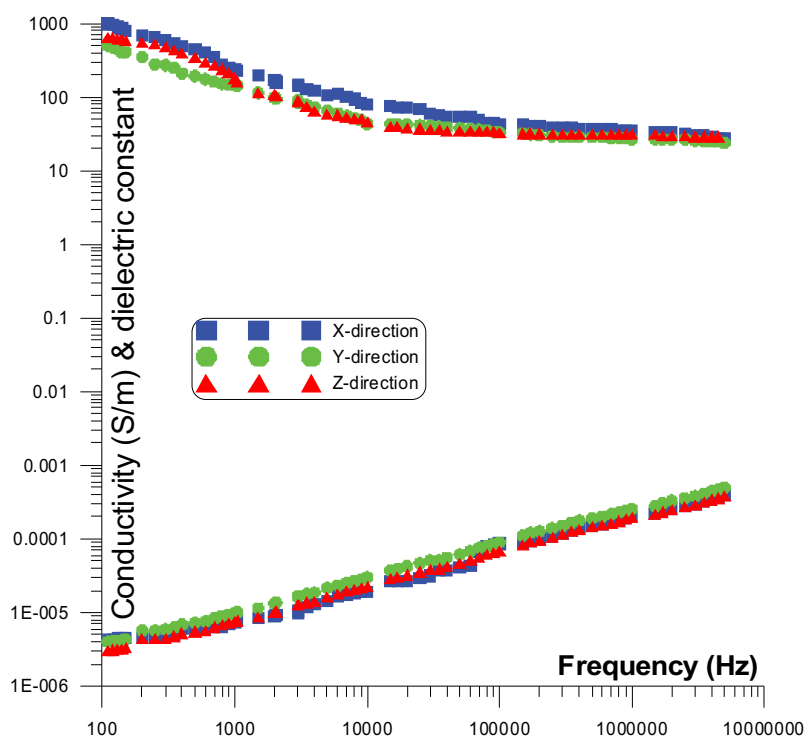


Figure 11. The conductivity and dielectric constant of pyrite sample (6) at three directions (X, Y and Z) of the crystal.

The general decrease of dielectric constant values, at specimens, with the raise of frequency and with the raise of total conductor concentration. This is due to raise of broken conduction paths (Shaltout et al. 2012, Abou Elanwar and Gomaa 2013). The existence of  $\text{SiO}_2$ , the main insulator concentration in samples, broke the continuous conductor paths. This will increase charge accumulation at ends of conducting links that will increase the dielectric constant. The average values of permittivity at three directions (X, Y and Z) are nearly identical (Figures 6,7,8,9,10, and figures 11). Accordingly, we can conclude that the samples are homogeneous. Also, the average changes of permittivity in each sample, for all samples, are so small and could be negligible when measured at three directions (X, Y and Z) of the crystal. Then, each sample is homogeneous (perfect cubic symmetry).

Most of samples behave as semiconductor even with the existence of relatively high values of  $\text{Fe}_2\text{O}_3$  because most of grains are dispersed and coated with the insulating grains.

The fluctuation present in conductivity and dielectric constant could be the result of variations at surfaces of each sample from the other (defects on the surface of cubic oxidised pyrite crystals).

All specimens show one slope with frequency for all curves. Particles or species may overcome barriers between energy levels to form continuous conductor paths between the grains when the frequency increases. According to that, the conductivity increases.

Oxidised Pyrite crystals are supposed to be a semiconductor whose electrical conductivity and dielectric constant are controlled by impurity content or trace elements, free charge carriers or crystal defects, thermal excitation across energy gaps and by their geochemical environment. We measured electrical features at three directions (X, Y, Z- dimensions). We intend to detect the homogeneity of crystals using electrical properties. When specimens are homogeneous then the electrical features at three directions (X, Y, Z- dimensions) will be similar. If specimens are not homogeneous, then the electrical features at three directions will be different. The change will be clear when there is a high change at grain shape and size of grains in a certain direction. The elongation of specimen grains in a certain direction will affect the electrical features and that will be an indication of homogeneity or heterogeneity of the specimen. Many electrically active impurities are present (cobalt, nickel, and copper) in cubic oxidised pyrite crystals. They may be donors or acceptors. There are many factors that influence charge carriers density at samples because cubic oxidised pyrite crystals occur in many types of environmental geology (Gomaa and Abou El-Anwar 2019). The nature of the solution, in

which the cubic oxidised pyrite crystals is immersed in it, determines the energy of pyrite. As mentioned before, the energy gaps of cubic oxidised pyrite crystals are nearly negligible at constant temperature (Shuey1975). There is a cubic symmetry in pyrite structure because the anionic species are present with identical numbers at each axes of cubic crystal (Abou El-Anwar and Gomaa 2013, 2016). From the samples, it is clear that there exists a range of electrical features for natural cubic oxidised pyrite crystals according to concentration of minor elements (Gomaa 2013). In the (Table 1), can be found Arsenopyrite (As), which has a tendency to have p-type semiconductor with relatively low conductivity. These observations may demonstrate the little and small changes between the different samples. Also, there is another factor that resulted from the different compositions of impurities in the different samples. There are some impurities of Cu (33 to 43) in cubic oxidised pyrite samples which means that the samples are created in sedimentary deposits with low hydrothermal temperature and that predominant conductivity is not the p-type (Shuey1975). The pyrite oxidation here may contain some As, Cu and Ni impurities with different concentrations (Shuey 1975) with some other impurities such as Ga, Pb and Zn. Electrical features of the cubic oxidised pyrite samples depend to a great extent on structural crystal defects that resulted from impurities like Fe or S (Rabinovich 1976; Schieck et al. 1990; Lehner et al. 2006). The substitution of Cu and Ni instead of Fe introduces occupied bulk defect conditions within the band gap that facilitate the transfer of electrons (Chandler and Bene 1973). Pyrite oxidation converts some ions in sulphate from  $\text{S}^{-1}$  to  $\text{S}^{6+}$ . The break of strong bonds between sulphur and iron produces thiosulphate ions which are relatively settled at alkaline electrolytes and unstable in acidic electrolytes.

## 5. Conclusion

Major, minor and rare earth element geochemical studies were accomplished on some cubic oxidised pyrite crystals (Gabal El-Sibai granites) samples. The chemical composition of samples shows that cubic oxidised pyrite crystals are essentially composed of  $\text{Fe}_2\text{O}_3$ ,  $\text{SiO}_2$ , and  $\text{Al}_2\text{O}_3$  with some trace and rare elements (Mn, Ba, Zr, Mo, Sr, Zn, Rb, Ni, Nb, Cu, Pb, U, Th, Ce, La, Nd, Sm and Y). Other minerals (haematite, goethite and arsenopyrite were detected by XRD, SEM. Fe, Si, Ba, Sr, La and Ce were measured by EDX. Detailed mineralogical, geochemical and electrical features studies were achieved on some of these cubic oxidised pyrite samples from southern part of Gabal El-Sibai granites. Electrical features were done at three (X, Y, and Z) dimensions of the cubic oxidised pyrite crystals within frequency range (100 Hz –5 MHz). Oxidised Pyrite crystals are homogeneous

and symmetric. Electrical features try to verify the homogeneity or heterogeneity (or anisotropy) of the cubic oxidised pyrite crystals. Slight variations exist in electrical features due to some imperfections at crystals with the existence of some different impurities at crystal surfaces. The electrical conductivity are controlled by impurity content, type, density of carrier and hence by their precipitation geochemical environment. Electrically, there exist many active impurities (cobalt, nickel, and copper) in pyrite. The conduction of pyrite is resulted from free charge carriers. Trace elements in solid solutions and thermal excitation across energy gaps are the sources of free charge carriers. Resistivity is inversely proportional concentration of charge carriers and their mobility. There are many electrically active impurities (As, Cu and Ni) in pyrite. The substitution of Cu and Ni instead of Fe introduces occupied bulk defects at band gaps which may facilitate electron transfer. The average values of conductivity for all specimens are identical and the average changes of values in electrical features in each sample are so small and could be negligible when measured at three directions. This indicates that each sample is homogeneous and there is no anisotropy at specimens because of perfect cubic symmetry at specimens. Dielectric constant decreases, generally, with increase of crystal defects, decrease of excitation along energy gaps that will increase broken conduction paths. The existence of SiO<sub>2</sub>, the main insulator concentration in samples, broke the continuous conductor paths. This will increase charge accumulation at the ends of the conducting links and accordingly increase the dielectric constant. The change of electrical features at three directions will be clear when there is a big variation at grain shape in a certain direction.


## Data availability

The raw/processed data required to reproduce these findings cannot be shared at this time as the data also forms part of an ongoing study. I hereby confirm that my paper is in accordance with the Journal guidelines.

## Disclosure statement

No potential conflict of interest was reported by the authors.

## ORCID

Mohamed Mahmoud Gomaa  <http://orcid.org/0000-0002-8556-4555>

## References

Abou El-Anwar E, Gomaa MM. 2016. Electrical, mineralogical, geochemical and provenance of Cretaceous black shales, Red Sea Coast, Egypt. *Egypt J Pet.* 25(3): pp.323–332. doi:10.1016/j.ejpe.2015.08.006.

- Abou El-Anwar EA, Gomaa MM. 2013. Electrical properties and geochemistry of carbonate rocks from the Qasr El-Sagha formation. El-Faiyum, Egypt, *Geophys Prospect.* 61(3):630–644. doi:10.1111/j.1365-2478.2012.01087.x.
- Abratis PK, Patrick RAD, Vaughan DJ. 2004. Variations in the compositional, textural and electrical properties of natural pyrite: a review. *Int J Miner Proc.* 74(1–4):41–59. doi:10.1016/j.minpro.2003.09.002.
- Ali MA. 2013. Mineral chemistry and genesis of Zr, Th, U, Nb, Pb, P, Ce and F enriched peralkaline granites of El-Sibai shear zone, Central Eastern Desert, Egypt. *Gija* 56/1, pp. 107–128.
- Börner JH, Girault F, Bhattarai M, Adhikari LB, Deldicque D, Perrier F, Spitzer K. 2018. Anomalous complex electrical conductivity of graphitic black schist from the himalayas of central. Nepal /*Geophys Res Lett.* 45 (9):3984–3993. doi:10.1029/2018GL077178.
- Butler CA, Dsworth RE, Stachan RA. 1995. Evidence for aledonian sinistral strikeslip motion and associated fault zone weakening, outer hebrides fault zone, NW Scotland. *J Geol Soc London.* 152(5):743–746. doi:10.1144/gsjgs.152.5.0743.
- Chandler RN, Bene RW. 1973. EPR study of the solid solutions Ni<sub>x</sub>Fe<sub>1-x</sub>S<sub>2</sub>, Co<sub>x</sub>Fe<sub>1-x</sub>S<sub>2</sub>, and Co<sub>x</sub>Ni<sub>y</sub>Fe<sub>1-x-y</sub>S<sub>2</sub>. *Phys Rev B.* 8(11):4979–4988. doi:10.1103/PhysRevB.8.4979.
- Chen H, Heidari Z. 2014. Pore-scale evaluation of dielectric measurements in formations with complex pore and grain structures, SPWLA 55th Annual Logging Symposium, Abu Dhabi, U.A.E., May 18–22.
- Clavier C, Heim A, Scala C. 1976. Effect of pyrite on resistivity and other logging measurements, SPWLA 17th Annual Logging Symposium, Denver, Colorado, June 9–12.
- Clennell MB, Josh M, Esteban L, Piane CD, Schmid S, Verrall M, McMullan B. 2010. The influence of pyrite on rock electrical properties: a case study from NW Australian gas reservoirs, SPWLA 51st Annual Logging Symposium, Perth, Australia, June 19–23.
- Craig JR, Vokes FM, Solberg TN. 1998. Pyrite: physical and chemical textures. *Mineral Deposita.* 34(1):82–101. doi:10.1007/s001260050187.
- Fedo M, Eriksson K, Krogstad J. 1996. Geochemistry of shale from the Archean (~ 3.0 Ga) buhwa Greenstone belt, Zimbabwe: implications for provenance and source area weathering. *Geochem SCosmic Acta.* 60 (10):1751–1763. doi:10.1016/0016-7037(96)00058-0.
- Fleischer M. 1955. Minor elements in some sulphide minerals. *Economic Geology*, 15th Anniversary, pp. 970–1024.
- Gomaa MM. 2009. Saturation effect on electrical properties of hematitic sandstone in the audio frequency range using non-polarizing electrodes. *Geophysl Prospect.* 57(6):1091–1100. doi:10.1111/j.1365-2478.2009.00797.x.
- Gomaa MM. 2013. Forward and inverse modeling of the electrical properties of magnetite intruded by magma, Egypt. *Geophys J Int.* 194(3):1527–1540. doi:10.1093/gji/ggt176.
- Gomaa MM, Abou El-Anwar E. 2019. Electrical, mineralogical, and geochemical properties of um gheig and um bogma formations, Egypt. *Carbonates Evaporites.* 34 (4):1251–1264. doi:10.1007/s13146-017-0370-5.
- Gomaa MM, Alikaj P. 2009. Effect of electrode contact impedance on a. c. electrical properties of wet hematite sample. *Mar Geophys Res.* 30(4):265–276. doi:10.1007/s11001-010-9092-y.



- Gomaa MM, Melegy A, Metwally H, Hassan S. 2020. Geochemical and electrical characterization of heavy metals in contaminated soils, Heliyon, Vol. 9, I6, In print.
- Greiling O, El-Ramly M, Rashwan A, Kamal El-Din GM. 1993. Towards a comprehensive structural synthesis of the (Proterozoic) Arabian Nubian Shield in E. Egypt. In: uthorweihe, schanDelMeie H, editor. Geoscientist Res. Northeast Africa. Rotterdam: Balkema; p. 15–19.
- Gurin G, Ilyin Y, Nilov S, Ivanov D, Kozlov E, Titov K. 2018. Induced polarization of rocks containing pyrite: interpretation based on X-ray computed tomography. J Appl Geophys. 154:50–63. doi:10.1016/j.jappgeo.2018.04.019.
- Kamal El Din GM. 1993. Geochemistry and tectonic significance of the pan-african el sibai window, central eastern desert, Egypt. Sci Series Int Bureau. 19:1–154.
- Kamal El-Din GM, 1991. Geochemistry and tectonic significance of the Pan-African El-Sibai window, Central Eastern Desert, Egypt. Ph. D. Thesis, Heidelberg University, 114.
- Lehner SW, Savage KS, Ayers JC. 2006. Vapor growth and characterization of pyrite (FeS<sub>2</sub>) doped with Co, Ni, and As: variations in semiconducting properties. J Crystal Growth. 286(2):306–317. doi:10.1016/j.jcrysgro.2005.09.062.
- MacLean W, Kranidiotis P. 1987. Immobile elements as monitors of mass transfer in hydrothermal alteration: phelps Dodge massive sulfide deposit. Matagami, Quebec Econ Geol. 82(4):951–962. doi:10.2113/gsecongeo.82.4.951.
- Misra S, Torres-verdín C, Homan D, Rasmus J, 2015. Complex electrical conductivity of mudrocks and source-rock formations containing disseminated pyrite. In Unconventional Resources Technology Conference, San Antonio, Texas, 20-22 July 2015 (pp. 2478–2490). Society of Exploration Geophysicists, American Association of Petroleum Geologists, Society of Petroleum Engineers.
- Pridmore DF, Shuey RT. 1976. The electrical resistivity of galena, pyrite, and chalcopryrite. Am Mineral. 61:248–259.
- Quinby-Hunt MS, Wilde P. 1994. Thermodynamic zonation in the black shale facies based on iron-manganese-vanadium conten. Chem Geol. 113(3–4):297–317. doi:10.1016/0009-2541(94)90072-8.
- Rabinovich KR. 1976. Relation of electrical properties with trace impurities in pyrites from quartz-gold ore deposits. Tr. Sib. Nauchno-Issled. Inst Geol Geofiz Miner Syr'ya. 236:31–36.
- Schieck R, Hartmann A, Fiechter S, Konenkamp R, Wetzel H. 1990. Electrical properties of natural and synthetic pyrite (FeS<sub>2</sub>) crystals. J Mater Res. 5(7):1567–1572. doi:10.1557/JMR.1990.1567.
- Shaltout AA, Gomaa MM, Wahbe M. 2012. Utilization of standard-less analysis algorithms using WDXRF and XRD for Egyptian Iron Ores identification. X-Ray Spectrom. 41(6):355–362. doi:10.1002/xrs.2410.
- Shannon RD. 1976. Revised effective ionic radii and systematic studies of interatomic distances in halides and chalcogenides. Acta Cryst. A32(5):751–767. doi:10.1107/S0567739476001551.
- Shen-Xubao H-Y, Iao-Tongpeng F-W, Hui-Qiangyao. 2008. Geochemistry of REE and yttrium in hydrothermal fluids from the Endeavour segment, Juan de Fuca Ridge. Geochem J. 42(4):359–370. doi:10.2343/geochemj.42.359
- Shuey RT. 1975. Semiconducting Ore Minerals. Amsterdam: Elsevier pub-lishing Co.
- Stern J, Hedge E. 1985. Gechronologic and isotopic constraints on Late Precambrian crustal evolution in the Eastern Desert in Egypt. Am J Sci. 258(2):97–12. doi:10.2475/ajs.285.2.97.
- Sultan M, Arvidson R, Duncan I, Stern J, El-Kalioubi B. 1988. Extension of the Najd shear system from Saudi Arabia to the central Eastern Desert of Egypt based on integrated field and Landsat observations. Tectonics. 7/6 (6):1291–130. doi:10.1029/TC007i006p01291.
- Taylor R, McLennan S. 1985. The continental crust: its composition and evolution. Oxford: Blackwell; p. 46–92.
- Yordanov Y, Kunov A. 1987. Geochemical behaviour of rare earth elements on metasomatic alteration of volcanic rocks. Comptes Rendus De l'Academie Bulgare Des Sciences. 40(5):77–80.